The 2009 IEEE/RSJ International Conference on
Intelligent Robots and Systems
October 11-15, 2009 St. Louis, USA

Microparticle Manipulation using Multiple Untethered Magnetic Micro-Robots on an Electrostatic Surface

Steven Floyd*, Chytra Pawashe*, and Metin Sitti

***Abstract*— This work presents the control of multiple untethered rectilinear magnetic micro-robots (Mag-μBots) with dimensions $250 \times 130 \times 100$ μm^3 actuated by pulsed external magnetic fields, which translate by induced stick-slip motion at speeds of up to 4 mm/s immersed in silicone oil. Multiple Mag-μBot control is enabled by employing an array of individually addressable electrostatic surfaces to selectively anchor individual Mag-μBots. Coupled parallel and uncoupled serial motion of multiple robots is demonstrated, and they can combine to form an assembly that is also capable of motion. Manipulation of 230 μm diameter microspheres is also demonstrated cooperatively by two Mag-μBots in a fluid environment, and is enhanced when the two Mag-μBots are combined. An analysis of the electrostatic anchoring forces and the forces relevant to manipulation is discussed.**

I. Introduction

The recent emergence of sub-millimeter sized mobile micro-robots has introduced new approaches to power delivery and control at the micron-scale. The current designs in literature, including electrostatic [1], [2], electromagnetic [3]–[7], laser driven thermal impact [8], and bacteria propelled systems [9], [10], have resulted in successful wireless control of individual micro-robots. These micro-robots are also capable of manipulating micron-scale objects in their respective workspaces. For example, Zhang et al. [4] demonstrate 6 μm spheres being manipulated by a micro-swimming flagellar device, and Frutiger et al. [5] show that 150 μm gold discs can be moved by a mobile micro-magnetic actuator. These approaches offer a valuable alternative to conventional micro-grippers controlled by a multi-degree-of-freedom macro-scale positioning system, which can be complex, difficult to control, and expensive [11]. In addition, such a system does not share the advantages of untethered micro-robots where the micron-scale end-effector is entirely contained within the workspace.

For any contact-based micro-manipulation method, stiction between the end-effector and micro-object becomes relevant at the micron-scale, making the release of grasped micro-objects difficult. Methods to combat this problem can include using ice to form and break connections between end-effectors and micro-objects, vibrating the end-effector to release a grasped object, employing vacuum to selectively capture and release micro-objects, and using electrostatic attraction and repulsion to manipulate micro-objects [12], [13]. Alternatively, the micro-object can be immersed in fluid, where micro-manipulation can be easier because stiction effects dramatically reduce. However, this limits applications to situations where the micro-object can be immersed, which is not always desired.

A new challenge in micro-robotics is the control of multiple untethered agents, where the power delivery and control mechanisms may not be conducive to this task. Donald et al. [1] demonstrate the control of four electrostatically actuated MEMS micro-robots, which are all designed to be physically different to respond differently to the global driving electric field. Motion among these micro-robots is coupled, and requires sophisticated algorithms to create paths for each micro-robot. Using magnetic-resonant micro-robots, Kratochvil et al. [6] demonstrate that decoupled motion is possible. Like in [1], these individual micro-robots must be physically different, so that their response to the global driving fields are unique.

To enable the control of multiple magnetic micro-robots (Mag-μBots) in our electromagnetically actuated system, we introduce a structured surface where electrostatic forces can be applied in order to selectively anchor Mag-μBots to the surface, which we demonstrate in [14]. This allows for any unanchored Mag-μBot to be driven by the encompassing magnetic fields, while keeping anchored Mag-μBots immobile. This approach allows for both the uncoupled serial actuation and coupled parallel actuation of multiple Mag-μBots. In this scheme, Mag-μBots do not need to be specially designed, reducing complexity of micro-robot fabrication.

Using Mag-μBots, the manipulation of microparticles can be performed within a fluid environment, which reduces the effects of stiction. In addition to forces exerted by the Mag-μBot by contact manipulation, fluid forces can also affect microparticles, caused by the displacement of fluid by the Mag-μBot while moving. This effect is explored in [15], where a single Mag-μBot can manipulate microparticles as small as 50 μm, limited by the imaging resolution of the system. The combination of multiple Mag-μBots and microparticle manipulation can lead to the vision of teams of micro-robots playing soccer, which is a goal for the RoboCup Nanogram league [16].

II. Tools and Concept

A rectilinear Mag-μBot with dimensions $250 \times 130 \times 100$ μm^3 is actuated by six independent electromagnetic coils, aligned to the faces of a cube approximately 11 cm on a

* Equally contributing co-first authors

S. Floyd and C. Pawashe are with the Department of Mechanical Engineering, Carnegie Mellon University, Pittsburgh, PA 15213, USA [srfloyd, csp]@andrew.cmu.edu

M. Sitti is with the Department of Mechanical Engineering and Robotics Institute, Carnegie Mellon University, Pittsburgh, PA 15213, USA sitti@cmu.edu

side, with horizontal and vertical coils capable of producing maximum field strengths at the position of the Mag-μBot of 3.0 mT and 2.3 mT, respectively (see Fig. 1). Imaging of the Mag-μBot and the workspace is accomplished by a camera (Sony XC-75) connected to a variable magnification microscope lens, providing an 8.6 mm $\times$ 7.2 mm field of view. Control of the electromagnetic coils is performed by a PC with a data acquisition system at a control bandwidth of 1 kHz, and the coils are powered by custom-made electronic amplifiers. The Mag-μBot is made of neodymium-iron-boron (NdFeB, N42 grade), a hard magnetic material. To create the robot, a magnetized piece of NdFeB was cut using a laser machining system (NewWave LaserMill).

Actuation of each Mag-μBot is accomplished by using two or three electromagnetic coils. One or more horizontal coils are first enabled (coil D in Fig. 1), causing the Mag-μBot to orient in the direction of the net magnetic field. The magnetic force exerted by the coils on the Mag-μBot is insufficient to translate it, due to friction and adhesion to the surface. Vertical clamping coils (coils C and F in Fig. 1) are enabled and pulsed using a sawtooth waveform, resulting in a non-uniform rocking motion of the Mag-μBot, which induces stick-slip motion across the surface. In general, the Mag-μBot's velocity increases with pulsing frequency, typically from 1-100 Hz, and can exceed velocities of 16 mm/s in air, and 4 mm/s in silicone oil, as used in this study. The Mag-μBot is also capable of operating in fluids of viscosities less than about 50 cSt, and can operate on a variety of smooth and rough magnetically inactive surfaces, provided that the adhesion between the Mag-μBot and surface is low. With an appropriate driving waveform, the Mag-μBot can be moved in steps down to about 5 μm.

Further details on this system are explained in [3], where modeling of the stick-slip dynamics is performed, and experimental analyses of robot motion is presented. Videos of operation can be found at [17], [18].

A. Multi-Robot Control

In Fig. 2, a schematic displaying the concept of multi-robot motion control is shown with four Mag-μBots. The Mag-μBots move on a grid surface, where each cell contains a set of interdigitated electrodes that provide electrostatic anchoring, and each cell is independently addressable [14]. To fabricate the surface, a silicon wafer is first coated with a 25 μm layer of SU-8. 100 nm of aluminum is then sputtered onto it, and patterned into the electrodes. A final layer of SU-8, approximately 1.5 μm thick, is coated onto the aluminum, and is in direct contact with the Mag-μBots. SU-8 is used for its high dielectric strength (112 V/μm), which supports the generation of the electric fields necessary to anchor a Mag-μBot without damaging the substrate. For experiments, a surface with 16 independent electrostatic pads in a 4×4 grid configuration was fabricated. Figure 3 displays a free body diagram of an anchored Mag-μBot with external electrostatic and magnetic forces, and a cross-section of the surface.

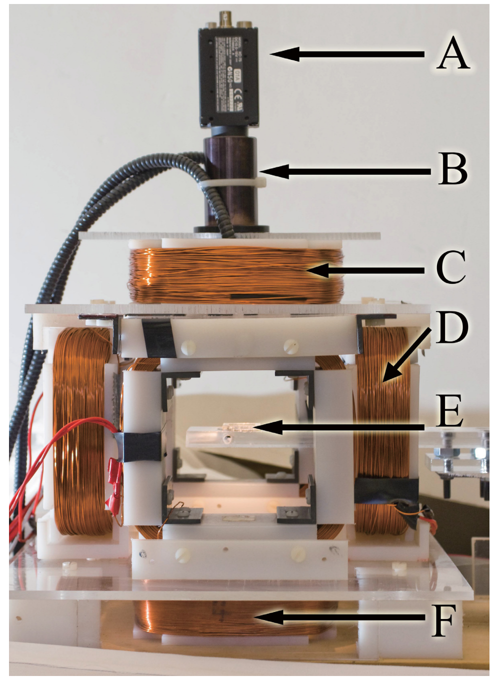

Fig. 1. Photograph of the electromagnetic coil setup, where A is the camera for visual feedback, B is the microscope lens, C is the top coil, D is one of four upright coils that orients the Mag-μBot within the plane on the surface, E is the surface on which the Mag-μBot locomotes, and F is the bottom coil. The top and bottom coils are clamping coils, which provide a clamping force and a torque that pushes and orients the Mag-μBot towards the surface, respectively.

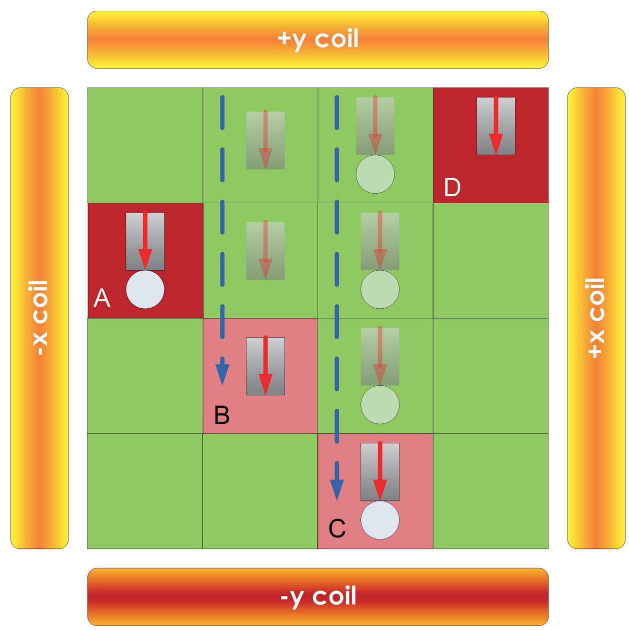

Fig. 2. Top-down schematic of four Mag-μBots, A, B, C, and D, demonstrating coupled and decoupled motion. The $-y$ coil is enabled, causing robots to orient in the $-y$-direction. Robots A and D are anchored to the surface and do not translate. Robots B and C translate in the $-y$-direction; robot B is anchored after having traversed one pad. Robot C pushes a microsphere during its travel.

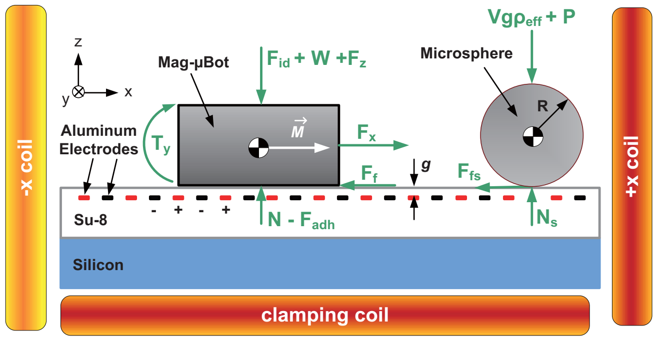

Fig. 3. Schematic of the Mag-μBot and a microsphere with magnetic, electrostatic, and gravitational forces and torques displayed. The Mag-μBot experiences an electrostatic anchoring force (F_{id}), its weight (W), magnetic forces (F_z and F_x), a magnetic torque (T_y), a static friction force (F_f), a reactive normal force (N), and an adhesive force (F_{adh}) due to surface effects. $\vec{M}$ denotes the magnetization vector of the Mag-μBot. When translating, forces on the microsphere include its effective weight ($Vg\rho_{eff}$), an adhesion force (P), a reactive normal force (N_s), and an immersed dynamic friction force (F_{fs}). The clamping and $+x$ coils are active. The composition of the electrostatic surface is also displayed.

III. Modeling

The Mag-μBot experiences electromagnetic, electrostatic, adhesive, and fluid forces from the environment. The effects of the electromagnetic forces are explained in detail in [3]. When a robot is anchored, the electrostatic force must prevent motion of the robot. To do this, it must prevent the robot from pivoting, which in turn prevents the stick-slip motion from occurring.

Microspheres in the workspace also experience these forces; magnetically inactive spheres, as used in this paper, will not respond to the magnetic fields. When each Mag-μBot is manipulating a microsphere, two interactions are of importance: the effects of adhesion and friction between the microsphere and the substrate, and the induced drag force on the microsphere from the fluid. The robot must be able to overcome both of these to successfully push microspheres. The effects of an electric field in the workspace can exert electrophoretic and dielectrophoretic forces on the microspheres. For the purposes of this paper, we ignore electrophoresis by assuming particles do not become charged while in the fluid, and assume that dielectrophoretic forces are negligible compared to fluid and contact forces, due to the relatively large microsphere sizes used.

This section provides the derivations of the relevant forces, and examines the conditions necessary for successful selective manipulation. The detailed effects of the fluid forces on limiting micro-robot velocity and allowing non-contact manipulation of micro-objects is covered in detail in [15].

A. Adhesion at the Micron-scale

When trying to pull two objects apart from one another, a non-zero pull-off force arises. This force is due to a combination of van der Waals interactions, capillary effects, and electrostatic charging [19]. Capillary forces can be neglected if the humidity is kept below 10%. Electrostatic effects are usually small compared to van der Waals effects due to the low dielectric strength of air [20]. To determine what the pull-off force for separating two materials 1 and 2 is, the work of adhesion, W_{12}, must be determined for the pair utilizing their intrinsic surface energies γ_1 and γ_2 [21], [22]:

$$W_{12} = \gamma_1 + \gamma_2 - \gamma_{12} \approx 2\sqrt{\gamma_1 \gamma_2}. \quad (1)$$

Adhesion modeling for micro and nanoparticle manipulation is discussed in [23], where the Johnson-Kendall-Roberts (JKR), Deraguin-Muller-Toporov (DMT), and Maugis-Dugdale (MD) models are explained. The range of possible pull-off forces, P, is curtailed and will fall within the range of:

$$\frac{3}{2}\pi R_e W_{12} \leq P \leq 2\pi R_e W_{12} \quad (2)$$

where the exact value of P can be determined based upon a variable called the elasticity parameter [22]. Hence, with only information on the surface energy of the material, an upper limit on P can be determined.

Values of several of these properties for different materials used in this work are given in Table I; the microspheres used are 230 μm diameter polystyrene divinylbenzene (PS-DVB, Duke Scientific Inc, properties assumed to be similar to polystyrene), and the fluid used is silicone oil (Dow Corning 200 fluid, 20 cSt).

Material	**Surface Energy** (γ) $[\mathrm{mJ \cdot m^{-2}}]$	**Density** (ρ) $[\mathrm{kg/m^{-3}}]$	**Dielectric Constant** (ϵ_r) -
SU-8	30-40 [24]	-	4.1
Polystyrene	33-40 [21], [25]	1060	-
Silicone oil	19.8-21 [26], [27]	935	2.3

TABLE I
Properties of Materials

Due to the range of possible surface energies for the materials in Table I, there is a large range of pull-off forces that can potentially exist for a polystyrene sphere of a given diameter on SU-8.

For irregularly shaped particles, the pull-off force will be greatly reduced from its perfectly smooth value, given in Eq. (2). To account for this, the irregularity can be quantified by treating the effective contact as a summation of several smooth spheres of varying radii:

$$P_{eff} = \sum_{i=1}^{N} \frac{3}{2}\pi R_i W_{12} = \frac{3}{2}\pi W_{12} \sum_{i=1}^{N} R_i. \quad (3)$$

If we assume that the number of contact points scales with the particle radius, and that the distribution of contact point radii is independent of the particle radius, then the summation term can be treated as an effective radius, $\sum_{i=1}^{N} R_i = R_{eff} = hR$, where $h \leq 1$. For highly irregular particles, $h \approx 0.1$ [28]. Using experimental data obtained from earlier work [29], the roughness of the polystyrene particles used in this work results in $h \approx 0.12$.

B. Adhesion in Fluid

When operating completely within a fluid, the capillary and electrostatic contributions to the pull-off force can be neglected. The van der Waals adhesion can be determined by taking into account the interactions with the fluid medium [22]:

$$W_{132} = W_{12} + W_{33} - W_{13} - W_{23} \tag{4}$$

where the subscripts 1 and 2 correspond to the solid materials, and 3 corresponds to the fluid medium.

In such a case, the resulting work of adhesion can be either positive or negative. Negative values imply the two surfaces repel each other, and the surfaces minimize their energy by contacting the fluid, not each other. For the range of values presented in Table I, the range for the immersed work of adhesion is $2.1\ \mathrm{mJ \cdot m^{-2}} < W_{132} < 6.9\ \mathrm{mJ \cdot m^{-2}}$. Taking into account particle irregularity, this translates into a range of pull-off forces of $180\ \mathrm{nN} < P_{eff} < 595\ \mathrm{nN}$.

C. Electrostatic Force

For the case of a conductive Mag-μBot above an SU-8 insulation layer covering a set of interdigitated electrodes at an applied voltage difference of V_{id}, the conductor will assume the mean potential if it overlaps equal areas of electrodes at both voltages [2]. With this assumption, the voltage difference between the Mag-μBot and each electrode will be $\frac{1}{2}V_{id}$. Assuming negligible fringing, an estimate of the anchoring force (F_{id}) exerted by the interdigitated electrodes onto the Mag-μBot is:

$$F_{id} = \frac{\epsilon_0 \epsilon_r}{8g^2} V_{id}^2 A_{id} \tag{5}$$

where A_{id} is the area of the Mag-μBot overlapping the electrodes, g is the insulator thickness, ϵ_0 is the permittivity of free space, and ϵ_r is the relative static permittivity of the insulating material (SU-8).

To anchor a Mag-μBot to the surface, the electrostatic force must suppress any Mag-μBot rotation about its contact point with the surface, caused by the magnetic torque, T_y. The effect of this torque significantly dominates all the other interactions experienced by the Mag-μBot, shown in Fig. 3. The maximum magnetic torque (T_{max}) that can be applied to a robot with a magnetization $\vec{M}$ at the maximum field strength $\vec{B}_{max}$ within this system is [3]:

$$T_{max} = \vec{M} \times \vec{B}_{max} \approx 2.88 \times 10^{-9}\ [\mathrm{N \cdot m}] \tag{6}$$

Treating the magnetic torque as a pair of forces acting in opposite directions on the ends of the Mag-μBot, each of these forces is approximately 11.6 μN. To counteract this, the anchoring force must be approximately twice this value, as it is evenly distributed across the bottom of the robot, and the torque about the pivot point will act at the center of the robot. Using Eq. (5) and noting that for electrodes that are 10 μm wide with 10 μm spacing, making A_{id} approximately half the apparent robot area of $A_{id} = 0.5 \cdot \left(250 \times 130\ \mu\mathrm{m}^2\right)$, the required voltage is approximately $V_{id} = 26$ V with g = 1.5 μm.

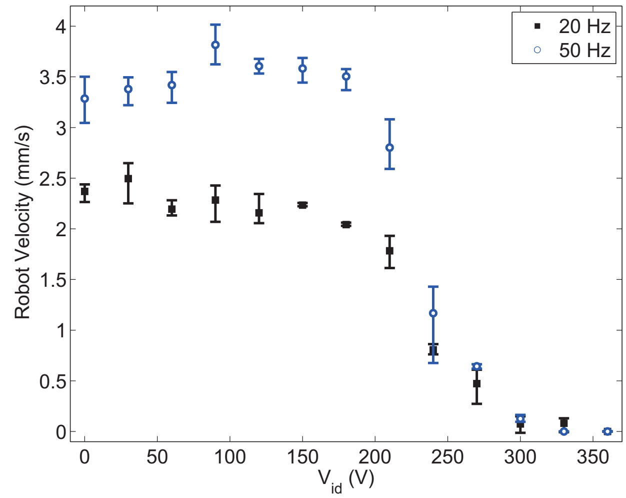

Fig. 4. Mag-μBot velocity vs. electrostatic anchoring voltage, V_{id}, at two pulsing frequencies on an SU-8 substrate with $g = 1.5\ \mu m$ in silicone oil. Each data point represents three experiments.

In Fig. 4 an experimental plot of Mag-μBot velocity vs. V_{id} is shown for two actuation frequencies. Velocity is measured by analyzing frames from a video of an experiment. As V_{id} increases from 0 V, the Mag-μBot's velocity slightly increases, particularly in the 50 Hz case; this can be due to an increased downward force causing the Mag-μBot to travel more during its slip phase (effectively adding to the magnetic clamping force). The Mag-μBot's velocity begins to decrease at $V_{id} = 180$ V, which is when the electrostatic anchoring force begins to dominate and detriments the slipping motion. The Mag-μBot completely stops at about $V_{id} = 360$ V; this high voltage requirement is likely caused by roughness on the Mag-μBot's surface, which can trap fluid beneath it and increase the separation from the electrodes. An additional fluid layer with thickness comparable to the robot's maximum asperity height of about $a = 10\ \mu$m, causes the total capacitance C_{tot} between the robot and the electrodes to be:

$$C_{tot} = \left(C_1^{-1} + C_2^{-1}\right)^{-1} \tag{7}$$

where C_1 is the capacitance associated with the SU-8 ($C_1 = \epsilon_0 \epsilon_{r1} g^{-1} A_{id}$) and C_2 is associated with the fluid gap ($C_2 = \epsilon_0 \epsilon_{r2} a^{-1} A_{id}$). Using the principal of virtual work and successive application of the chain rule for differentiation, the electrostatic anchoring force with a fluid gap ($F_{id,fg}$) will be:

$$F_{id,fg} = \frac{1}{16} V_{id}^2 C_{tot}^2 \left[\frac{1}{C_1 g} k + \frac{1}{C_2 a}(1-k)\right] A_{id} \tag{8}$$

where k is a constant ($0 < k < 1$) relating the amount of virtual SU-8 displacement that occurs per unit of total virtual displacement. Taking the limit when k = 0 and all the contraction is in the fluid gap, 257 V is required to anchor the robot. When k = 1 and all the contraction is in the SU-8, 343 V is required. This range is slightly lower than the experimentally determined voltage of 360 V. Minor fabrication defects such as poorly formed electrodes, variations in insulation thickness, resistive losses in the electrodes, and variations in the roughness of the robots can cause the required voltage to increase.

D. Manipulation Capabilities

Using the information in the previous sections, logical limits can be determined on the Mag-μBot's ability to push a microsphere based upon the forces that must be overcome. Within a fluid medium, there exists a minimum lateral force, F_{min}, to move an object:

$$F_{min} \approx \mu_f \left[2\pi R W_{132} + (\rho_p - \rho)Vg\right] \tag{9}$$

where μ_f is the immersed friction coefficient between the surface and the object. For the case of a 230 μm sphere, 18 nN $< F_{min} <$ 59 nN if it is assumed $\mu_f = 0.1$.

The maximum possible forces exerted by the Mag-μBot can be roughly estimated as the maximum lateral magnetic force that can be applied to the Mag-μBot, approximately 52 nN [3]. Hence, if the immersed friction coefficient is much larger than 0.1, or if the surface energies of SU-8 and polystyrene are near the high end of their ranges, pushing with a single robot will be difficult, if not impossible.

IV. Results and Discussion

To demonstrate the control of multiple Mag-μBots with the electrostatic anchoring surface, three Mag-μBots were placed on the surface within silicone oil, which supports the generation of the electric anchoring fields and enables microsphere manipulation due to reduced stiction effects. An electrostatic potential of V_{id} = 400 V was used to anchor the Mag-μBots.

In Fig. 5, three Mag-μBots are displayed, where uncoupled serial motion and coupled parallel motion are both demonstrated. In addition the Mag-μBots assemble and are able to translate while assembled; qualitatively, this Mag-μBot structure translates at higher velocities than each individual Mag-μBot.

In Fig. 6, two Mag-μBots are displayed with four 230 μm diameter PS-DVB microspheres. Each of the Mag-μBots takes turns pushing the spheres in a serial fashion. The two Mag-μBots then assemble and the combined structure is capable of pushing spheres as well.

From these experiments, the electrostatic anchoring surface is capable of preventing Mag-μBot motion. In most cases however, anchored Mag-μBots will change in orientation due to the encompassing magnetic field. This occurs because the relatively strong magnetic torque exerted on the Mag-μBot overcomes any additional friction to the surface caused by anchoring. This friction is derated due to the fact that the Mag-μBot's surfaces are rough, causing adhesion to the surface to decrease. In some cases the Mag-μBot remains fixed in orientation, e.g. R_b in Fig. 5c-d, possibly due to a relatively smooth surface on this particular Mag-μBot.

When two Mag-μBots become sufficiently close to each other, they jump-into contact due to the high magnetic field gradients caused by their magnetization. This jump-into distance implies that there is a minimum distance two Mag-μBots must maintain between each other to ensure successful individual motion, and is experimentally about 2-3 body lengths (500-750 μm) within fluid. This distance can be reduced by designing robots with lower magnetizations. Assembled Mag-μBots are still capable of translating, as the fundamental stick-slip dynamics have not changed. Translational speeds observed are higher with this structure because the magnetic forces and torque scale with volume, while the viscous drag and surface adhesion scale only with area.

Microsphere manipulation is performed by the Mag-μBots; however some microspheres tend to stick to the substrate more than others, and as a result, individual Mag-μBots are sometimes incapable of moving them (as in Fig. 6b). When the Mag-μBots combine into larger assemblies, the total pushing force also increases, which allows previously stuck microspheres to be pushed (see Fig. 6d).

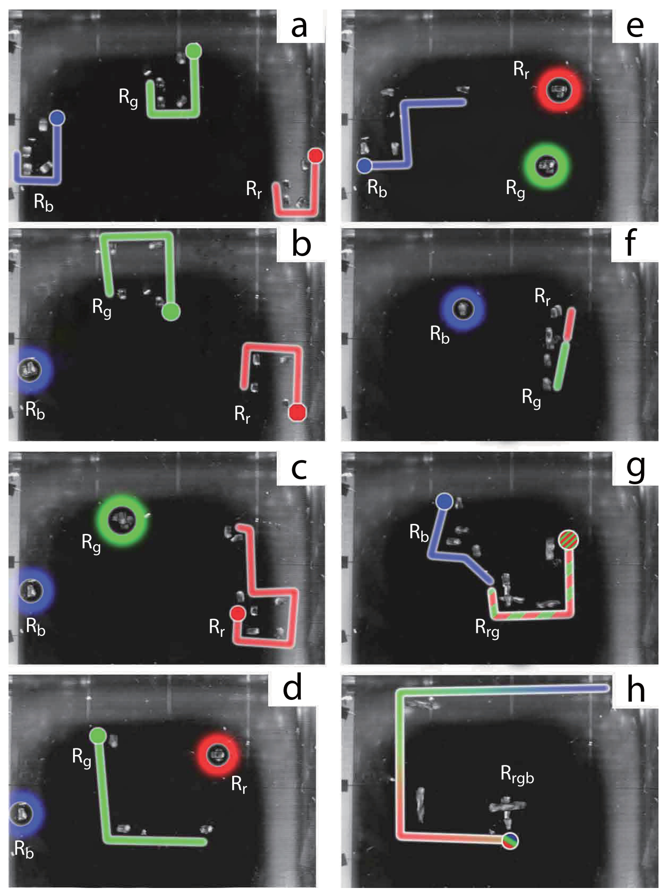

Fig. 5. (Color online) Frames from a movie with three Mag-μBots, R_r (red), R_g (green), and R_b (blue), traversing individually and in parallel under silicone oil. In (a) all three robots move identically, in (b) R_b is anchored and R_g and R_r move, in (c) R_g becomes anchored and R_r moves, in (d) only R_g is free to move, in (e) only R_b is free to move, in (f), R_r and R_g combine into R_{rg}, in (g) R_{rg} moves to combine with R_b, and in (h) all robots combine into R_{rgb} and move. Circles indicate Mag-μBot starting position. Total experiment time is 43 sec. Noise and dust were digitally removed from frames for clarity. Videos are available at [18].

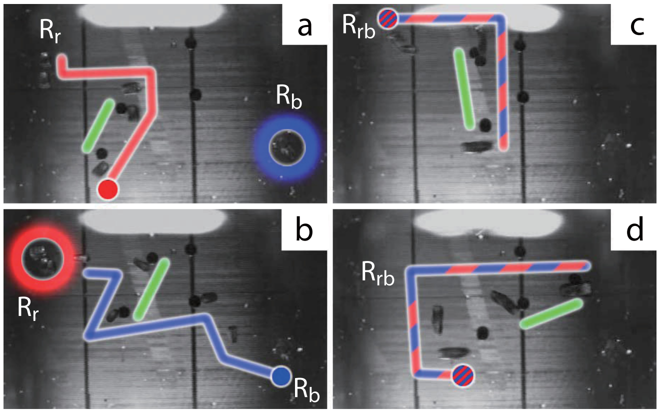

Fig. 6. (Color online) Frames from a movie with two Mag-μBots, R_r (red) and R_b (blue), manipulating 230 μm PS-DVB microspheres (green) under silicone oil. In (a) R_b is anchored and R_r pushes a microsphere upwards, in (b) R_r is anchored and R_b pushes a microsphere upwards after failing to push a stuck microsphere, in (c) the two Mag-μBots assemble to form R_{rb} and push a microsphere downwards, and in (d) R_{rb} pushes the previously stuck microsphere to the right. Circles indicate Mag-μBot starting position. Total experiment time is 50 sec. Videos are available at [18].

V. CONCLUSIONS

In this study, we demonstrate that multiple untethered magnetic micro-robots with dimensions 230 $\times$ 130 $\times$ 100 μm^3 can move both in parallel, and individually with decoupled motion. This capability was enabled by an array of 16 independent electrostatic anchoring pads on the substrate. Pushing of microspheres was also demonstrated within a fluid with two Mag-μBots, and is a step towards team-based micron-scale soccer for the RoboCup Nanogram League.

Models describing the electrostatic forces were given to quantify the anchoring behavior of the electrostatic pads on a Mag-μBot, and experimental results displayed the required electrostatic voltages. Models for estimating the required force to push microspheres are also presented.

Future works will include incorporating vision and path planning algorithms to autonomously control multiple Mag-μBots to perform tasks such as microparticle assembly. Mag-μBots with lower magnetization will also be investigated to decrease jump-into contact distances and allow disassembly.

ACKNOWLEDGMENT

The authors would like to thank the NanoRobotics Laboratory members for all of their support and suggestions. This work is supported by the National Science Foundation CAREER award program (NSF IIS-0448042), and the NSF Graduate Research Fellowship.

REFERENCES

[1] B. Donald, C. Levey, and I. Paprotny, "Microassembly by Parallel Actuation of MEMS Microrobots," Journal of Microelectromechanical Systems, Vol. 17, No. 4, pp. 789-808, 2008.

[2] B. Donald, C. Levey, C. McGray, D. Rus, M. Sinclair, "Power Delivery and Locomotion of Untethered Microactuators," Journal of Microelectromechanical Systems, Vol. 12, No. 6, pp. 947-959, 2003.

[3] C. Pawashe, S. Floyd, and M. Sitti, "Modeling and Experimental Characterization of an Untethered Magnetic Micro-Robot," International Journal of Robotics Research, 2009, in press.

[4] L. Zhang, J. J. Abbott, L. Dong, B. E. Kratochvil, D. Bell, and B. Nelson, "Artificial bacterial flagella: Fabrication and magnetic control," Applied Physics Letters, Vol. 94, No. 064107, 2009.

[5] D. R. Frutiger, K. Vollmers, B. E. Kratochvil, and B. J. Nelson, "Small, fast, and under control: wireless resonant magnetic micro-agents," International Symposium on Experimental Robotics, Athens, Greece, 2008.

[6] B. E. Kratochvil, D. Frutiger, K. Vollmers, and B. J. Nelson, "Visual Servoing and Characterization of Resonant Magnetic Actuators for Decoupled Locomotion of Untethered Mobile Microrobots," IEEE International Conference on Robotics and Automation, Kobe, Japan, 2009.

[7] A. Yamazaki, M. Sendoh, K. Ishiyama, K. I. Arai, R. Kato, M. Nakano, H. Fukunaga, "Wireless micro swimming machine with magnetic thin film," Journal of Magnetism and Magnetic Materials, Vol. 272-276, pp. e1741-e1742, 2004.

[8] O. Sul, M. Falvo, R. Taylor, S. Washburn, R. Superfine, "Thermally Actuated Untethered Impact-driven Locomotive Microdevices," Applied Physics Letters, Vol. 89, No. 203512, 2006.

[9] S. Martel, C. Tremblay, S. Ngakeng, and G. Langlois, "Controlled manipulation and actuation of micro-objects with magnetotactic bacteria," Applied Physics Letters, Vol. 89, No. 233904, 2006.

[10] B. Behkam and M. Sitti, "Bacterial flagella-based propulsion and on/off motion control of microscale objects," Applied Physics Letters, Vol. 90, No. 023902, 2007.

[11] D. Popa and E. Stephanou, "Micro and Meso Scale Robotic Assembly," J. Manufacturing Processes, Vol. 6, No. 1, pp. 52-71, 2004.

[12] J. Abbott, Z. Nagy, F. Beyeler, and B. Nelson, "Robotics in the Small, Part I: Microrobotics," IEEE Robotics and Automation Magazine, Vol. 14, No. 2, pp. 92-103, June 2007.

[13] M. Sitti, "Microscale and nanoscale robotics systems - Characteristics, state of the art, and grand challenges," IEEE Robotics and Automation Magazine, Vol. 14, No. 1, pp. 53-60, March 2007.

[14] C. Pawashe, S. Floyd, and M. Sitti, "Multiple magnetic microrobot control using electrostatic anchoring," Applied Physics Letters, Vol. 94, No. 164108, 2009.

[15] S. Floyd, C. Pawashe, and M. Sitti, "Two-Dimensional Contact and Non-Contact Micro-Manipulation in Liquid using an Untethered Mobile Magnetic Micro-Robot," IEEE Transactions on Robotics, 2009, in press.

[16] See online: http://www.nist.gov/public_affairs/calmed/robocup_photos.html

[17] Available online: http://nanolab.me.cmu.edu/

[18] Available online: http://ieeexplore.ieee.org/

[19] R. Fearing, "Survey of Sticking Effects for Micro Parts Handling," IEEE/RSJ Int. Conf. on Intelligent Robots and Systems, Vol. 2, pp. 212-217, 1995.

[20] F. Arai, D. Ando, T. Fukuda, Y. Nonoda, and T. Oota, "Micro Manipulation Based on Micro Physics - Strategy Based on Attractive Force Reduction and Stress Measurement," IEEE/RSJ Int. Conf. on Intelligent Robots and Systems, vol. 2, pp. 236-241, 1995.

[21] M. Gauthier, S. Regnier, P. Rougeot, N. Chaillet, "Forces Analysis for Micromanipulations in Dry and Liquid Media," Journal of Micromechatronics, vol. 3, no. 3-4, pp. 389-413, 2006.

[22] J. Israelachvili, "Intermolecular and Surface Forces," Academic Press, London, 1992.

[23] M. Sitti and H. Hashimototo, "Teleoperated Touch Feedback from the Surfaces at the Nanoscale: Modeling and Experiments," IEEE/ASME Transactions on Mechatronics, vol. 8, no. 1, pp. 287-298, 2003.

[24] C. Chung and Y. Hong, "Surface Modification of SU8 Photoresist for Shrinkage Improvements in a Monolithic MEMS Microstructure," J. Micromechanics and Microengineering, Vol. 17, pp. 207-212, 2007.

[25] M. Yuce and A. Demirel, "The Effect of Nanoparticles on the Surface Hydrophobicity of Polystyrene," European Physics Journal B, Vol. 64, pp. 493-497, 2008.

[26] See online: http://www.surface-tension.de/solid-surface-energy.htm

[27] F. Heslot, A. Cazabat, P. Levinson, and N. Fraysse, "Experiments on Wetting on the Scale of Nanometers: Influence of the Surface Energy," Physical Review Letters, Vol. 65, No. 5, pp. 599-602, 1990.

[28] D. Quesnel, D. Rimai, and L. Sharpe, "Particle Adhesion: Applications and Advances," Taylor and Francis, 2001.

[29] Pawashe, C., and Sitti, M., "Two-Dimensional Vision-Based Autonomous Microparticle Manipulation using a Nanoprobe," Journal of Micromechatronics, 3(3-4): 285-306, July 2006.